

Identifying crack initiation and propagation thresholds in brittle rock

E. Eberhardt, D. Stead, B. Stimpson, and R.S. Read

Abstract: Recent work at the Underground Research Laboratory of Atomic Energy of Canada Limited in Pinawa, Manitoba, has shown that high compressive stresses near the tunnel face significantly contribute to the loss of strength, and eventual failure of the rock, through stress-induced brittle fracturing. A program of laboratory testing has been undertaken to investigate the effects of brittle fracture on the progressive degradation of rock mass strength. The work carried out in this study involves a detailed analysis of the crack initiation and propagation thresholds, two key components in the brittle-fracture process. This paper describes new techniques developed to enhance existing strain gauge and acoustic emission methodologies with respect to the detection of these thresholds and their effects on the degradation of material strength.

Key words: tunnel, rock failure, brittle fracture, crack initiation, crack propagation.

Résumé : Des travaux récents au «Underground Research Laboratory» de l'AECL à Pinawa, Manitoba, ont démontré que les fortes contraintes de compression près de la face du tunnel contribuent de façon significative à la perte de résistance, et éventuellement à la rupture de la roche, par suite de fractures fragiles induites par les contraintes. Un programme d'essais en laboratoire a été entrepris pour étudier les effets de la fracture fragile sur la dégradation progressive de la résistance de masse de la roche. Le travail réalisé dans cette étude comprend une analyse détaillée de l'initiation de la fissure et des seuils de propagation, deux composantes clés dans le processus de la fracture fragile. Cet article décrit de nouvelles techniques qui ont été développées pour valoriser les méthodologies existantes de jauges de contraintes et d'émission acoustique pour la détection de ces seuils et de leurs effets sur la dégradation de la résistance du matériau.

Mots clés : tunnel, rupture de la roche, rupture fragile, initiation de fissures, propagation de fissures.

[Traduit par la rédaction]

Introduction

The excavation of an underground opening in a stressed rock mass results in the deformation of the near-field rock due to a redistribution of stresses, resulting in induced stress concentrations. This stress redistribution increases strain energy in zones of increased compression. If the resulting imbalance in the energy of the system is severe enough, it can result in the progressive degradation of the rock mass strength through fracturing. Thus it is important to establish the thresholds associated with microscale and macroscale fracturing in the in situ rock mass.

The deformation and fracture characteristics of brittle rock have been studied by numerous researchers over the past 30 years (Brace 1964; Bieniawski 1967a; Wawersik and Fairhurst 1970; Lajtai and Lajtai 1974; Martin and Chandler

1994). The general consensus of these studies has been that the failure process can be broken down into a number of stages based largely upon the stress-strain characteristics displayed through axial and lateral deformation measurements recorded during uniaxial and triaxial laboratory tests. Based on the stress-strain behaviour of a loaded material (Fig. 1), Brace (1964) and Bieniawski (1967a) defined these stages as being (1) crack closure, (2) linear elastic deformation, (3) crack initiation and stable crack growth, (4) critical energy release and unstable crack growth, and (5) failure and postpeak behaviour.

Crack closure occurs during the initial stages of loading ($\sigma < \sigma_{cc}$ in Fig. 1, where σ is the total axial stress and σ_{cc} is the stress at crack closure) when preexisting cracks orientated at an angle to the applied load close. During crack closure, the stress-strain response is nonlinear, exhibiting an increase in axial stiffness (i.e., deformation modulus). The extent of this nonlinear region is dependent on the initial crack density and geometrical characteristics of the crack population. Once the majority of preexisting cracks have closed, linear elastic deformation takes place. The elastic constants (Young's modulus, Poisson's ratio) of the rock are calculated from this linear portion of the stress-strain curve.

Crack initiation (σ_{ci}) represents the stress level where microfracturing begins and is marked as the point where the lateral and volumetric strain curves depart from linearity. Crack propagation can be considered as being either stable or unstable. Under stable conditions, crack growth can be stopped by controlling the applied load. Unstable crack growth occurs at the point of reversal in the volumetric strain curve and is also known as the point of critical energy release or crack damage

Received July 24, 1998. Accepted December 2, 1997.

E. Eberhardt.¹ Department of Geological Sciences, University of Saskatchewan, Saskatoon, SK S7N 5E2, Canada.

D. Stead. Camborne School of Mines, University of Exeter, Redruth, Cornwall TR15 3SE, England.

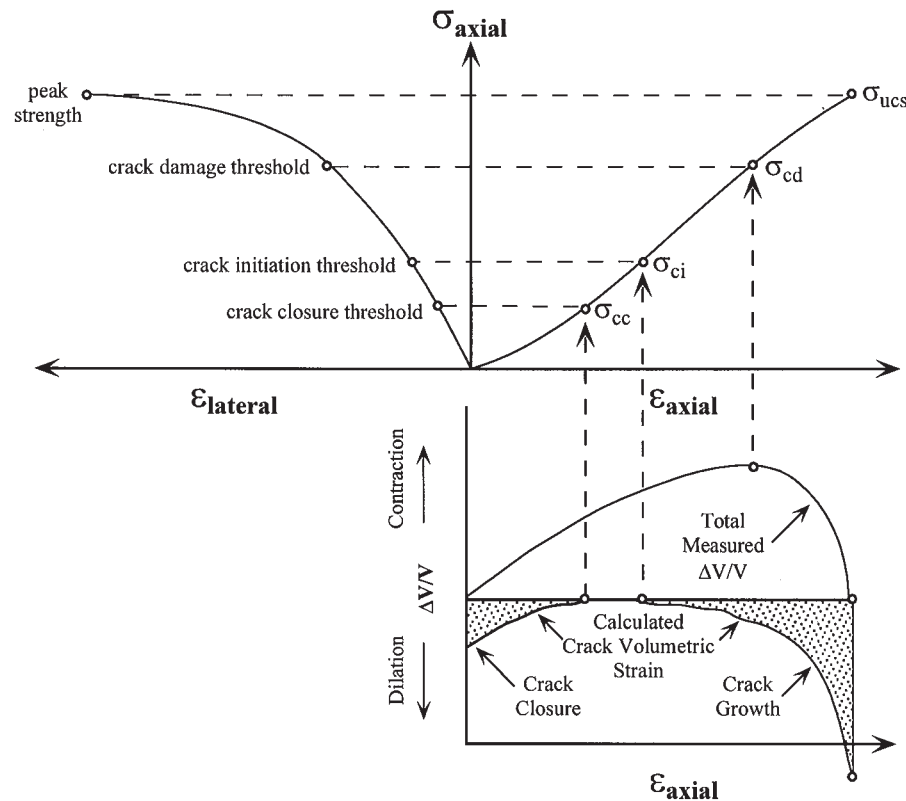
B. Stimpson. Department of Civil and Geological Engineering, The University of Manitoba, Winnipeg, MB R3T 5V6, Canada.

R.S. Read.² Whiteshell Laboratories, Atomic Energy of Canada Limited, Pinawa, MB R0E 1L0, Canada.

¹ Present address: Engineering Geology, ETH Hönggerberg, 8093 Zürich, Switzerland.

² Present address: Klohn-Crippen Consultants Ltd., Calgary, AB T2E 7H7, Canada.

Fig. 1. Stress–strain diagram showing the elements of crack development (after Martin 1993). Note that only the axial (ϵ_{axial}) and lateral ($\epsilon_{\text{lateral}}$) strains are measured; the volumetric strain and crack volume are calculated. σ_{axial} , axial stress; σ_{ucs} , peak strength; ΔV , change in volume; V , initial volume.



stress threshold σ_{cd} (Martin 1993). Bieniawski (1967a) defines unstable crack propagation as the condition which occurs when the relationship between the applied stress and the crack length ceases to exist and other parameters, such as the crack growth velocity, take control of the propagation process. Under such conditions, crack growth would continue even if the applied load were kept constant.

Unstable crack growth continues to the point where the numerous microcracks have coalesced and the rock can no longer support an increase in load. Martin (1993) notes that the peak strength of granite (including the uniaxial compressive strength in unconfined tests) is not a unique material property but is dependent on loading conditions such as the loading rate. The crack initiation and crack damage stresses were found to be more characteristic, essentially independent of loading conditions.

Work at the Atomic Energy of Canada Limited (AECL) Underground Research Laboratory (URL) has concentrated on using the crack initiation (σ_{ci}) and crack damage (σ_{cd}) stress thresholds to better quantify rock damage. The detection of these thresholds, however, has proven difficult especially with respect to crack initiation. A series of uniaxial tests were subsequently performed to refine existing analysis techniques for determining the crack initiation stress threshold of intact rock. These techniques involve the use of stress–strain data and acoustic emission monitoring. New methods of data analysis were also introduced to help substantiate the interpretation of the data with respect to crack initiation and growth. These methods include the application of a moving point regression technique to the stress–strain data and an exami-

nation of the changes in the acoustic event properties with loading. Testing was performed on cylindrical samples of Lac du Bonnet granite obtained from the URL 130 Level (130 m below ground surface). This paper examines the effects of crack initiation and damage in the degradation of material strength, emphasizing the underlying mechanisms and characterization methods.

Detection of crack development in brittle rock

A number of techniques have been developed to detect and study crack growth in brittle materials. The most common of these involves the use of electric resistance strain gauges to measure slight changes in sample deformation that can be related to the closing and opening of cracks (Brace et al. 1966; Bieniawski 1967b). To a lesser extent, acoustic emission monitoring has been used to correlate the number of acoustic events to various strain gauge responses (Scholz 1968; Ohnaka and Mogi 1982; Khair 1984). Other techniques have involved the use of photoelastics, optical diffraction patterns, scanning electron microscopes, laser speckle interferometry, ultrasonic probing, and electrical resistivity.

Stress–strain data

Strain gauge measurements have provided the most insight into delineating the stages of crack development in rock. The use of strain gauges in past studies, however, has been somewhat limited by data sampling, computing, and storage

capabilities. Recent work by the Rock Mechanics Research Group at the University of Saskatchewan has been directed towards using more powerful computers with larger data storage capabilities in conjunction with faster data logging systems. These capabilities have allowed for tests to be conducted in which the sampling rate has been increased five to ten times that allowable with older testing systems (i.e., capable of five measurements per second). Thus more data points along the axial and lateral stress-strain curves can be collected and examined for indications of crack growth. In essence, higher resolution of sample deformation relating to crack initiation and growth is achieved.

Moving point regression technique

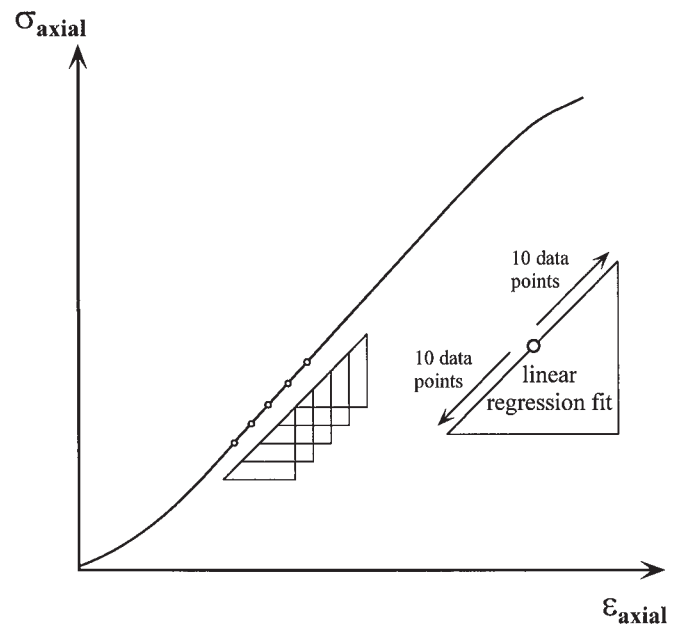
Improvements can also be made in the way strain gauge data are analyzed. Stress-strain data analysis has traditionally concentrated on picking noticeable slope changes in the plotted stress-strain curves (axial, lateral, and calculated volumetric) which may then be correlated to several of the theoretical stages in crack development. However, a high degree of error and subjectivity is incorporated into this analysis procedure when one considers the combined use of poor data resolution and the manual picking of points. Bearing in mind that certain inflections, some of which may be undetectable to the unaided eye, in the stress-strain curves are of key interest, a moving point regression technique, which uses the first derivative of the curves to highlight any slope or rate changes in the curves, was developed.

The moving point regression technique uses a "sliding window" approach to move through an x , y data set, fitting a straight line over a user-defined interval. The slope at each point is calculated over the interval and recorded, the process being repeated at successive points (Fig. 2). When plotted against the parameter of interest, inflections in the original x , y data curve are highlighted. For example, using an axial stress versus axial strain curve, the technique produces a moving point average of the changes in the Young's modulus throughout loading (Fig. 3). This is referred to as the average axial stiffness, therefore avoiding problems in terminology when calculating the slope outside the range of linear elastic behaviour. In regards to the sensitivity of the method to the user-defined regression interval, it was found that the general shape of the stiffness curve remained the same with increasing interval sizes, but small-scale fluctuations in the measured deformation response were filtered out when extremely large regression intervals were used. Analysis results indicate that the size of the regression interval should be approximately 5% of the total number of x , y data pairs.

Acoustic emission response in rock

Acoustic emission (AE) in polycrystalline rock originates as a result of dislocations, grain boundary movement, or initiation and propagation of fractures through and between mineral grains. The sudden release of stored elastic strain energy accompanying these processes generates an elastic stress wave which travels from the point of origin within the material to a boundary where it is observed as an acoustic event (Hardy 1977). AE techniques have been used with some success in identifying microfracturing in brittle materials. Scholz (1968) found that characteristic AE patterns in rock correlate closely with stress-strain behaviour. However, most of the success in

Fig. 2. Moving point regression technique.



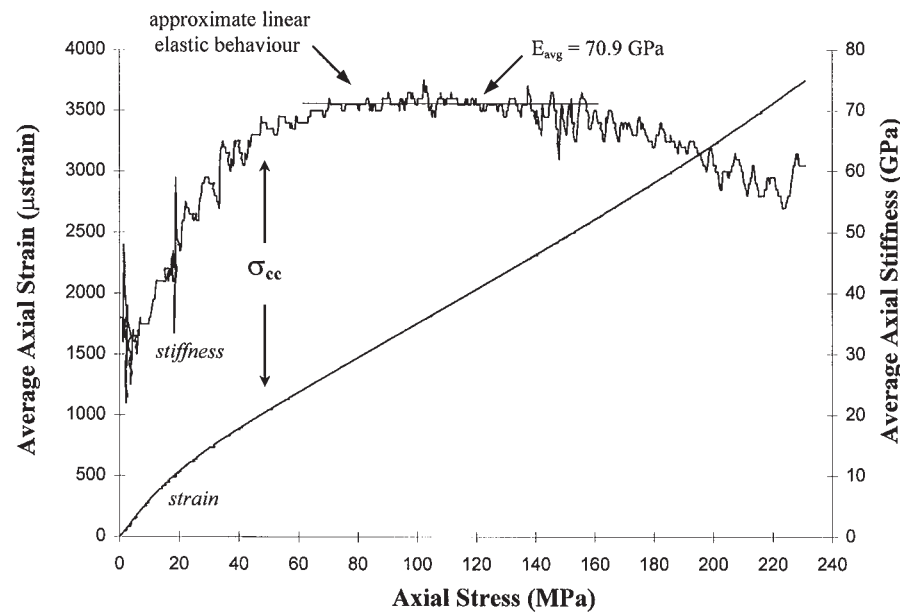
correlating AE activity to microfracturing has involved the later stages of crack development. This is due to the fact that the majority of AE events occur just prior to failure. The lack of significant AE activity in the initial stages of loading makes it more difficult to distinguish background noise from fracture-related acoustic events. A balance must be struck between setting event threshold limits high enough to filter out the majority of the background noise, yet low enough to pick up the beginning of the microfracturing process.

Characteristics of an acoustic event

In addition to recording the number of acoustic events and correlating this number to the measured deformation response in the rock, it is also possible to record certain properties of the AE waveforms. The signal waveform of an acoustic event is affected by the characteristics of the source, the path taken from the source to the sensor, the sensor characteristics, and the recording system. Generally, these waveforms are complex and using them to characterize the source can be difficult. Due to these complexities, AE waveform analysis can range from simple parameter measurements to more complex pattern recognition. However, relatively little work has been done in the area of waveform analysis with respect to rock mechanics and the progressive degradation-failure process in rock.

The event threshold serves as a reference for several of the simple waveform parameters (Fig. 4). These AE event properties are defined in Table 1. The characteristics of an acoustic event may also be used to approximate the release of kinetic energy through the AE event. The true energy is directly proportional to the area under the acoustic emission waveform which in turn can be measured by digitizing and integrating the waveform signal. However, this can be both difficult and time consuming. As a simplification, the event energy can be approximated as the square of the peak amplitude (Spanner et al. 1987; Lockner et al. 1991) or the square of the peak amplitude multiplied by the event duration (Beattie 1983; Mansurov 1994). The resulting values are actually more

Fig. 3. Moving point regression analysis of axial stress–strain data showing the changes in axial stiffness throughout loading for a 130 Level pink granite. E_{avg} , average Young’s modulus.



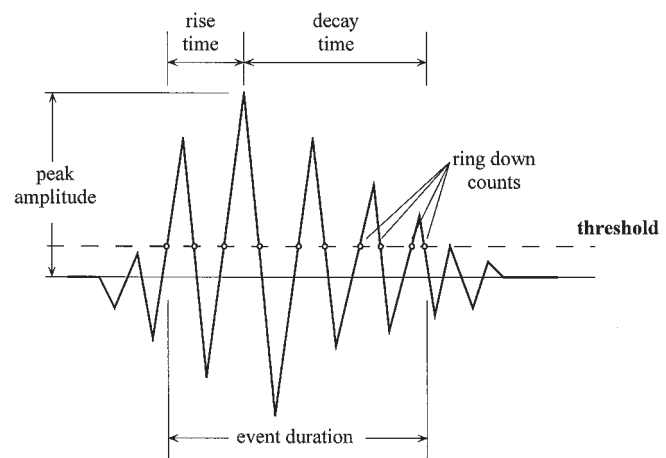
representative of the event power (the units are given in dB and dB-s, respectively), but are commonly referred to as energy calculations in the literature due to their approximately linear relationship with energy. This type of “energy” analysis helps in accentuating AE events with abnormally large amplitudes or durations.

Laboratory testing of Lac du Bonnet granite

Laboratory uniaxial testing was performed on 20 samples of pink Lac du Bonnet granite from the 130 Level of the URL. The pink granite is medium to coarse grained, with an average grain size between 3 and 4 mm. Based on work by Jackson and Lau (1990), 61 mm diameter cores were chosen to minimize size effects. Jackson and Lau found that samples of Lac du Bonnet granite with smaller diameters were more sensitive to sample disturbance, thereby influencing the observed mechanical behaviour of the rock samples during testing.

Samples were prepared for testing according to American Society for Testing and Materials standards (designation ASTM D4543-85) with length to diameter ratios of approximately 2.25. Considerable care was taken in minimizing the influence of end effects on strain gauge and AE transducer readings. This entailed the use of a specially constructed frame that allowed for the sample ends to be highly polished. Measurements of end surface flatness and perpendicularity five times lower than those recommended by ASTM standards were attained. Each sample was instrumented with six Micro-Measurement electric resistance strain gauges (three axial and three lateral at 60° intervals, 12.7 mm in length, with a 5% strain limit) to record sample deformation and four 175 kHz piezoelectric transducers to record acoustic emissions. Strain gauges were epoxied directly to the cleaned sample surface to ensure a solid bond, whereas the AE transducers were mounted onto wave guides, which were in turn epoxied

Fig. 4. Definition of simple acoustic emission waveform parameters.



to the sample surface. Acoustic emissions were recorded with an AET 5500 logging system using a gain of 40 dB and a threshold value of 0.1 V.

Prior to uniaxial testing, P - and S -wave traveltimes were recorded for each sample (Table 2). Results from these measurements indicate a significant increase (40–50%) in both P - and S -wave velocities when compared with previously tested granite and granodiorite samples from the 420 Level of the URL (Eberhardt et al. 1996). With maximum in situ stresses increasing from approximately 15 MPa at 130 m depth to 60 MPa at 420 m depth (Martin 1990), considerable damage through stress-induced microcracking would be expected in samples from the 420 Level. Static elastic properties were determined from the stress–strain data following ASTM standards (designation D3148-93) and include Poisson’s ratio, average Young’s modulus, and secant Young’s modulus (Table 3). The difference between the average and secant modulus

Table 1. Definition of acoustic emission (AE) event properties (as shown in Fig. 4).

AE event property	Description
Ring-down count	The number of times a signal crosses a preset threshold datum; in general, large events require more cycles to ring down to the threshold level and will produce more counts than a smaller event; provides a measure of the intensity of the acoustic emission event
Peak amplitude	Related to the intensity of the source in the material producing an AE event; measurements are generally recorded in logarithmic units (decibels dB) to provide accurate measurement of both large and small signals
Event duration	When an acoustic event first crosses the preset threshold, an event detector measures the time that the waveform amplitude remains above the threshold, thereby giving the event duration
Rise time	Measures the time it takes to reach the peak amplitude of an event; provides an account of the positive-changing AE signal envelope

Table 2. Average acoustic velocities of URL granites.

Location rock type	Density (g/cm ³)	P wave (m/s)	S wave (m/s)
130 Level pink granite	2.62 (±0.01)	4890 (±190)	3030 (±120)
420 Level grey granite	2.61 (±0.02)	3220 (±100)	2160 (±60)

Note: Standard deviation is given in parentheses.

Table 3. Average static elastic moduli for URL pink granite at the 130 Level.

Property	130 m Level Pink Granite
Average modulus, E_{avg} (GPa)	66.1 (±2.5)
Secant modulus, E_s (GPa)	61.0 (±2.9)
Poisson's ratio, ν	0.31 (±0.04)

Note: Standard deviation is given in parentheses.

(which would include any nonlinearity due to preexisting cracking) for the 130 Level samples is relatively small (5 GPa), indicating that initial sample damage is relatively low.

Interpretation of crack development in Lac du Bonnet granite

It is generally accepted that the first fractures in a uniaxially loaded brittle material are tensile microcracks (Lajtai and Lajtai 1974). The growth of these cracks has been shown to occur in the direction of the major principal stress (σ_1), where cracks not aligned with σ_1 grow along a curved path to align themselves with σ_1 (Fig. 5). This phenomenon has been observed in a number of materials including glass (Brace and Bombolakis 1963; Hoek and Bieniawski 1965), hard plastics (Nemat-Nasser and Horii 1982; Cannon et al. 1990), plaster (Lajtai 1971), ice (Schulson et al. 1991), and rock (Wawersik and Fairhurst 1970; Peng and Johnson 1972; Huang et al. 1993). The opening of crack faces parallel to the applied load and the closure of crack faces perpendicular to the load cause certain changes in the relative lateral and axial deformations, respectively. These changes appear as inflections in the stress-strain curves which, in turn, can be used to identify the different stages of rock deformation and failure.

Test results were analyzed to define the stages of rock deformation and failure as defined by Brace (1964) and Bieniawski (1967a). The following discussion highlights some of the key observations. Results from this analysis are summarized in Table 4.

Crack closure

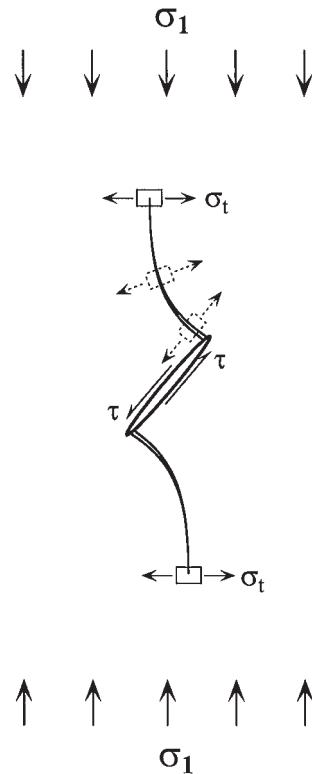
The crack closure stress level (σ_{cc} in Fig. 1) indicates the load at which a significant number of preexisting cracks have closed and near-linear elastic behaviour begins. This point is approximated by determining the point on the stress-strain curve where the initial axial strain appears to change from nonlinear to linear behaviour. Crack closure stresses (σ_{cc}) were picked for each test using the moving point regression analysis (Fig. 3). As was expected, a rapid increase in axial stiffness was observed before values levelled off and behaved in a relatively linear manner. This pattern and the corresponding values were consistent for each test (Table 4).

Examination of the lateral stiffness curve (Fig. 6) over this region reveals relatively high stiffness values when the load is first applied to the sample (the lateral stiffness term, although somewhat unconventional, represents the change in the lateral strain rate with axial loading). Artificially high values of this term during the initial stages of loading represent a point in the load history where there is not a continuous transmission of stresses due to the presence of open microcracks, therefore the lateral and axial strain responses are not fully coupled. These initially high values are followed by a marked reduction (35%) during the first 25 MPa of loading. The initial stages of crack closure appear to predominantly involve the simple movement of preferentially aligned crack walls towards one another, parallel to the direction of applied load. This would have a significant effect on the axial strain but little effect on the lateral strain, since the displacement would be in the axial direction. With increasing load, values of lateral stiffness begin to rapidly decrease, possibly signifying shear or sliding movement between the faces of closing or closed cracks. This behaviour has been observed in glass plates by Bieniawski (1967b) who noted that the sliding deformation demonstrated by single closed cracks continues even during linear elastic behaviour.

Linear elastic behaviour

Figure 3 shows that after crack closure is reached, a period of relatively linear axial strain occurs. The average Young's

Fig. 5. Model of internal crack extension towards the major principal stress. σ_1 , major principal stress; τ , shear stress.



modulus was taken as a least squares fit along this region. In terms of lateral stiffness, linear behaviour is never truly reached. Instead, the lateral stiffness continuously decreases from values of approximately 300 GPa to values less than 20 GPa prior to failure (Fig. 6). This would seem to indicate that a number of processes may be contributing towards the gradual but continual loss of lateral stiffness in the specimens tested. These may include sliding (shear) between faces of closing cracks, tensile opening of cracks during crack initiation, and possibly further shear movement related to crack coalescence – columnar buckling during the latter stages of rock deformation. Following ASTM standards, Poisson’s ratio was calculated using a least squares fit over the same interval as that used in calculating the average Young’s modulus (i.e., linear region of the axial stress–strain curve). It will be shown later that this may not be the most appropriate interval over which to calculate Poisson’s ratio.

Crack initiation

The crack initiation stress threshold, as determined through laboratory testing, has been defined as the point where the lateral strain curve departs from linearity (Brace et al. 1966; Bieniawski 1967a; Lajtai and Lajtai 1974). Examination of the lateral strain curve (Fig. 6) reveals that the identification of this point can be very subjective. This is clear from analysis of the lateral stiffness curve which indicates that at no time is the lateral stress–strain curve truly linear. Noting the difficulty in using lateral strain gauge data, especially in highly damaged samples, Martin (1993) suggested using the calculated crack volumetric strain to identify crack initiation. For a cylindrical sample loaded uniaxially, crack volume is determined by sub-

Table 4. Average strength parameters for URL pink granite.

Property	Stress threshold (MPa)
Crack closure, σ_{cc}	47.5 (± 2.9)
Crack initiation, σ_{ci}	81.5 (± 3.7)
Crack coalescence, σ_{cs}	104.0 (± 3.8)
Crack damage, σ_{cd}	157.3 (± 9.9)
Peak strength, σ_{ucs}	206.5 (± 10.0)

Note: Standard deviation is given in parentheses.

tracting the linear elastic component of the volumetric strain, given by

$$[1] \quad \epsilon_{V_{\text{elastic}}} = \frac{1 - 2\nu}{E} \sigma_{\text{axial}}$$

where E and ν are the elastic constants and σ_{axial} is the axial stress level, from the volumetric strain calculated from the measured axial (ϵ_{axial}) and lateral ($\epsilon_{\text{lateral}}$) strains, given by

$$[2] \quad \epsilon_V = \epsilon_{\text{axial}} + 2\epsilon_{\text{lateral}}$$

The remaining volumetric strain is attributed to axial cracking, i.e.,

$$[3] \quad \epsilon_{V_{\text{crack}}} = \epsilon_V - \epsilon_{\text{elastic}}$$

Martin (1993) defines crack initiation as the stress level at which dilation (crack volume increase) begins in the crack volume plot (Fig. 1).

This method is limited, however, because of its dependence on the use of the elastic constants E and ν . Although the Young’s modulus E can be determined with a reasonably high degree of confidence and consistency, the nonlinearity of the lateral strain response complicates the measure of Poisson’s ratio. The resulting value is the ratio of lateral to axial strain magnitudes based on the linear elastic axial strain behaviour and the “best approximation” of a straight line through a non-linear region of lateral strain over the same stress interval. Table 5 lists the respective Poisson’s ratio values calculated over the same stress interval as the average Young’s modulus (as per ASTM standards) and over the stress interval between crack closure and crack initiation as determined using the moving point regression analysis. This variability introduces a large degree of uncertainty into the crack volume calculation used to determine crack initiation. Figure 7 demonstrates the sensitivity of crack initiation values to changes in the Poisson’s ratio using crack volume reversal as the indicator (for example, a change of ± 0.05 in the Poisson’s ratio results in a $\pm 40\%$ change in the σ_{ci} value). The crack volume stiffness plot shown in Fig. 7 is calculated as the change in slope of the crack volume strain curve, the reversal of which is noted by the change from a positive to a negative slope.

Using an approach that involved the combined use of the moving point regression analysis and acoustic emission response, it was found that the crack initiation stress threshold could be more accurately determined. From the strain gauge data, it was found that, although the lateral strain is nonlinear, rate changes do occur and can be correlated to the growth of cracks in the sample. These rate changes are most evident when analyzing the volumetric strain and stiffness curves (Fig. 8). The volumetric stiffness curve is based on the stress-dependent rate of change in the volumetric strain. Volu-

Fig. 6. Plots of lateral strain and lateral stiffness against axial stress for a 130 Level pink granite.

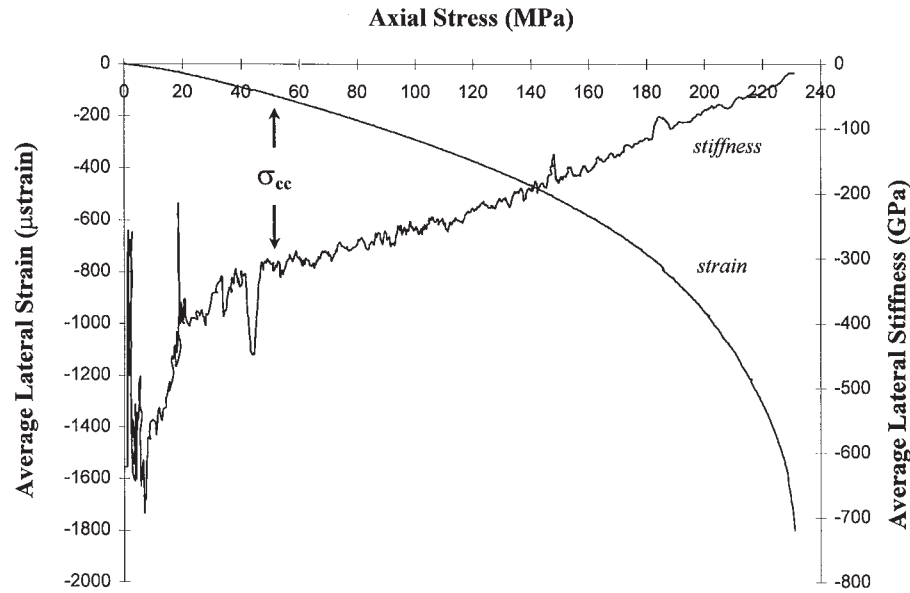
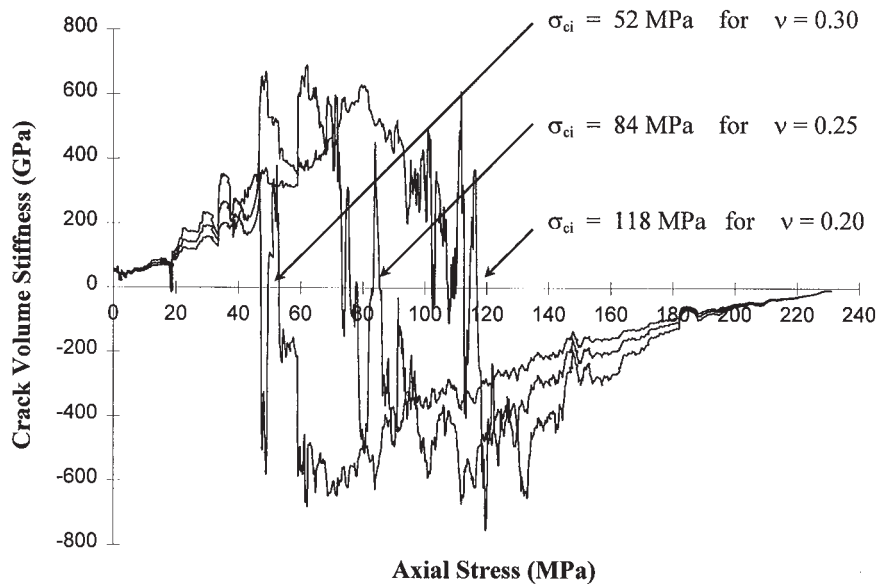


Fig. 7. Variability of crack volume strain reversal with Poisson's ratio for a 130 Level pink granite.



metric strain is defined in eq. [2]. The volumetric stiffness is calculated as the slope of the volumetric strain versus axial stress curve. The rate at which the volumetric strain curve changes is dependent on the rate of change in the measured axial and lateral strain.

Examination of the volumetric stiffness curve indicated a series of characteristic patterns (Fig. 8) that recur in each of the uniaxial tests performed. During the initial stages of loading, the axial strain controls the shape of the volumetric strain curve. The nonlinear behaviour of the axial strain during crack closure distinguishes itself as an irregular region along the volumetric stiffness curve (Fig. 9). This irregular region is followed by a linear region marked by a small break in slope signifying a rate change. This break in slope represents the transition from crack closure to near-linear elastic behaviour. This linear region also marks the stress interval in which the

lateral strain achieves its most linear behaviour (i.e., the Poisson's ratio should be calculated in this region as shown in Table 5). The volumetric stiffness curve then makes a transition to a less regular region without any discernible break in slope at approximately 80 MPa. Throughout this region the axial strain rate maintains a near-constant level, therefore any change can be attributed to a change in the lateral strain rate. Changes in the lateral strain rate result in slight slope changes in the volumetric strain curve. However, because the axial strain rate still dominates in controlling the shape of the volumetric strain curve, no noticeable slope change occurs in the volumetric stiffness curve. Although these changes in the lateral strain rate do not contribute to the overall volumetric strain enough to cause a major change in the slope of the volumetric stiffness curve, they do contribute enough to cause irregularities in it. These changes in the lateral strain rate, and conse-

Fig. 8. Plots of volumetric strain and volumetric stiffness against axial stress for a 130 Level pink granite.

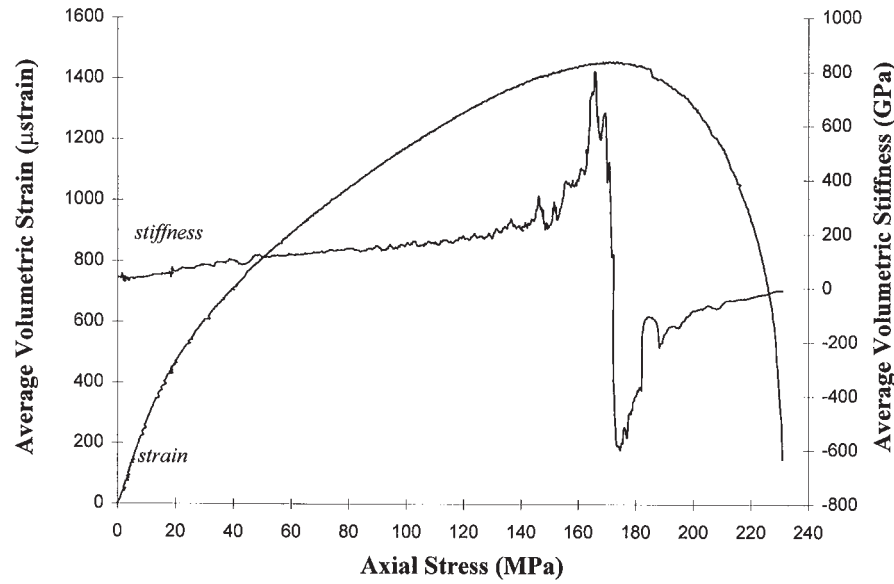


Fig. 9. Breakdown and correlation of volumetric stiffness with the stages in the compressive failure process of rock for a 130 Level pink granite.

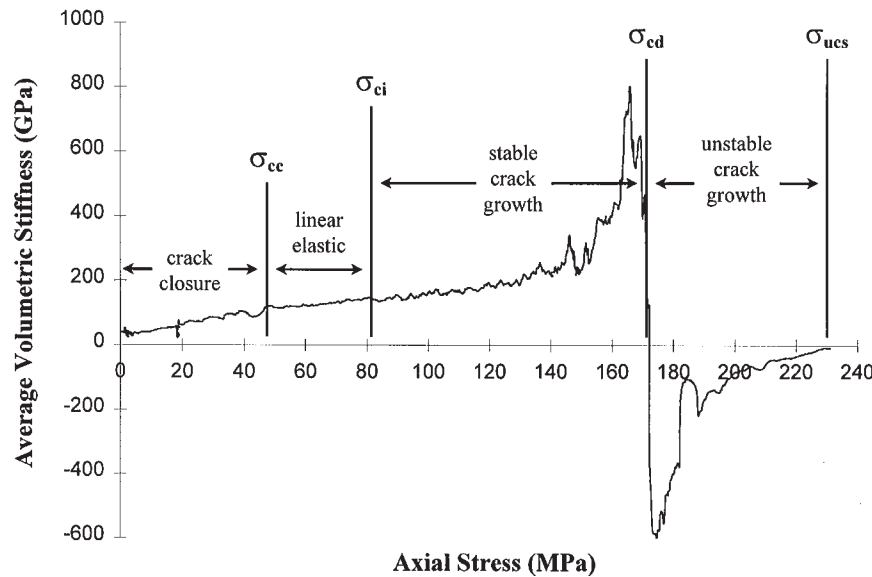


Table 5. Average Poisson’s ratio ν for URL pink granite at the 130 Level.

Method of calculation	ν
ASTM ^a	0.31 (± 0.04)
$\sigma_{cc} \rightarrow \sigma_{ci}$ ^b	0.24 (± 0.03)

Note: Standard deviation is given in parentheses.

^a Calculated according to ASTM standards.

^b Calculated over the stress interval between crack closure and crack initiation as determined through the moving point regression analysis.

quently the volumetric stiffness curve, signify crack initiation at approximately 80 MPa.

Correlation between the behaviour of the volumetric stiffness curve and crack initiation can also be validated through acoustic emission analysis. The average response from the four AE transducers shows that the majority of activity occurs towards the end of the test. Although AE activity occurs continuously throughout the test, the logarithmic plot in Fig. 10 shows that the beginning of significant AE activity is at approximately 80 MPa. This coincides with the crack initiation stress threshold (σ_{ci}) of 80 MPa as determined using the volumetric stiffness curve in Fig. 9. AE activity prior to this point can be attributed to movement along crack faces during crack closure, as recognized in the lateral strain rate and previously discussed. It is also likely that small cracks may form during low stresses in areas already weakened by stress-relief cracking.

Fig. 10. Plot of log acoustic emission event count vs. axial stress for a 130 Level pink granite.

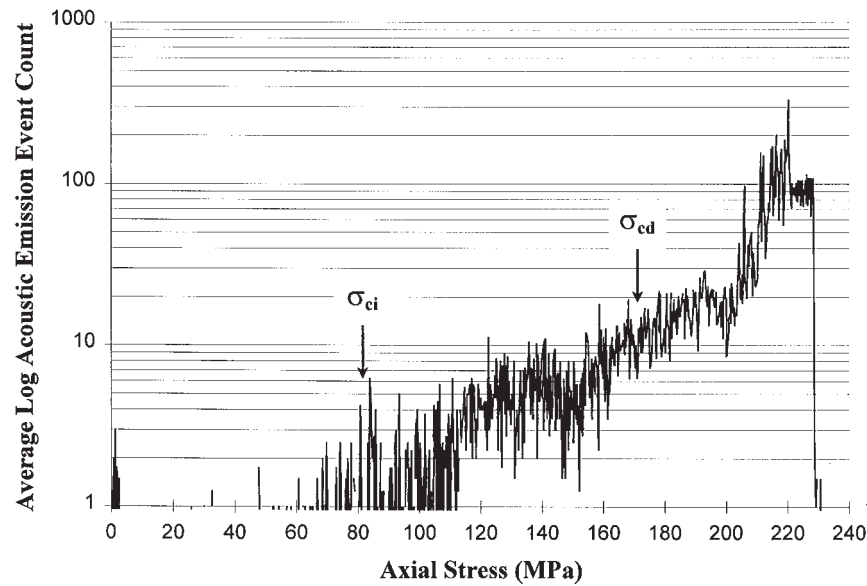
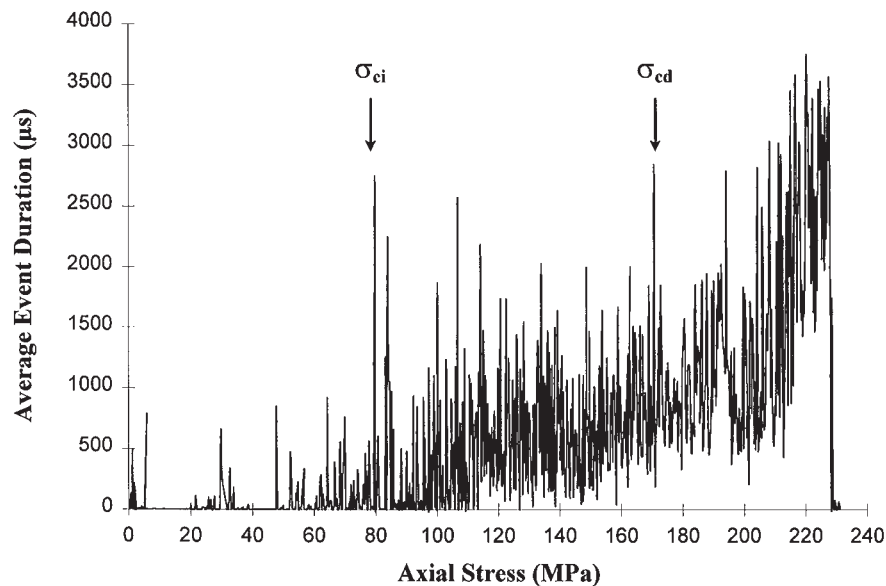


Fig. 11. Plot of event duration vs. axial stress for a 130 Level pink granite.



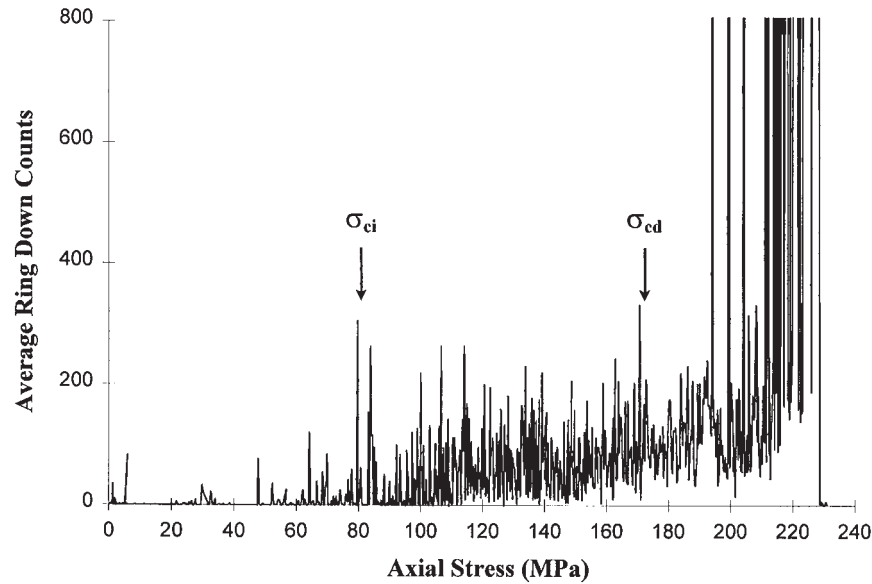
In addition to the acoustic emission response, the properties of the acoustic events themselves are markedly different before and after crack initiation. Figures 11 and 12 contain plots of the maximum event duration and ring down counts. From these plots it can be seen that a marked increase in their respective magnitudes occurs at approximately 80 MPa, coinciding with crack initiation. Larger event durations and ring down counts both signify larger acoustic events. Although acoustic activity occurs prior to this point, the size of the events is relatively small (in terms of event duration, these events are 70% shorter in duration than those occurring above 80 MPa). This may indicate that the acoustic events generated through crack closure are much smaller than those generated through stress-induced tensile cracking. Calculations of the acoustic event "energy" based on the peak amplitude and event duration of the event waveform (herein referred to as the elastic impulse energy so as not to confuse it with the true energy) also rein-

forces these observations. Plots of the elastic impulse energy and its stress-dependent rate change (Fig. 13) show that the size of the events in terms of energy dramatically increases shortly after crack initiation begins.

Crack coalescence and crack damage

In defining the various stages of crack behaviour, stable crack growth is interpreted as one stage bounded at the lower end by the crack initiation stress threshold (σ_{ci}) and at the upper end by the crack damage stress threshold (σ_{cd}). Analysis of laboratory data, however, indicates that this region may consist of two stages distinguished by a major change in the volumetric strain rate. Analysis of both the axial and lateral stiffness curves indicates that a large rate change occurs in strain well before unstable crack propagation (i.e., σ_{cd}). During stable crack growth, rate changes are believed to occur solely in terms of lateral strain, since crack growth is predominantly in

Fig. 12. Plot of ring down counts vs. axial stress for a 130 Level pink granite.



the direction of uniaxial loading (i.e., σ_1). Volumetric strain reversal then occurs as a result of increases in the lateral strain rate surpassing the constant axial strain rate as the dominant component in the volumetric strain calculation. This results in a reversal of the volumetric strain curve defining the crack damage threshold. Analysis indicates, however, that the axial stiffness is not constant but decreases well before σ_{cd} at 160 MPa (Fig. 3). Analysis confirms that the lateral strain rate change does eventually exceed the rate change in axial strain thereby causing the reversal in the volumetric strain curve. These changes can be seen in the volumetric stiffness curve, where large increases in the lateral strain rate combined with changes in the axial strain rate cause large irregularities as the volumetric strain curve approaches reversal (Fig. 14).

The unexpected departure from linear behaviour seen in the axial strain response prior to the crack damage threshold may be explained through the coalescence of propagating cracks in a loaded sample. At the beginning of crack initiation, small tensile cracks begin to grow parallel to the applied load. These cracks originate from small flaws preferentially aligned to the loading direction so as to induce cracking through high tensile stress concentrations. The cracks are assumed to appear randomly throughout the sample and, for the most part, are isolated from one another. They have very little effect in decreasing the overall competency of the rock. As the load is increased additional cracks begin to grow as their individual strengths are exceeded, incrementally contributing to the degradation of the inherent rock strength (i.e., cohesion). This is evident in the acoustic emission data which show increasing bursts of AE activity leading up to σ_{cd} (Fig. 10).

As cracks increase, both in number and size, they eventually begin to interact with one another. Crack interaction then becomes extremely complex as stress shadows overlap. This has been demonstrated using a numerical modelling study of the process (Eberhardt et al. 1998). Eventually cracks will begin to step out and coalesce (i.e., develop en echelon (Lajtai et al. 1994)). This coalescence of cracks would involve some crack growth at oblique angles to the loading direction and

perhaps an element of shearing, thereby contributing to a change in the axial strain rate. Thus, the changes seen in the axial and volumetric stiffness curves may be attributed to a stage of crack coalescence (σ_{cs}) prior to the crack damage stress threshold.

Following crack coalescence, determination of the crack damage stress threshold (σ_{cd}) is relatively straightforward. Although a certain degree of subjectivity may be introduced by picking the point of volumetric strain reversal directly off the volumetric strain curve, the point stands out very clearly in a plot of volumetric stiffness versus axial stress (Fig. 14). The crack damage threshold could represent the intermediate-term strength of the sample, since beyond this point failure will eventually occur through unstable cracking (Martin 1993). Values of σ_{cs} and σ_{cd} for the tested samples are given in Table 4.

Conclusions

The deformation and fracture characteristics of brittle rock are an important consideration in assessing its long-term strength. The initiation, propagation, and interaction of stress-induced cracks are closely linked but extremely complicated. Through the combined use of strain gauge analysis and acoustic emission monitoring, techniques were developed to aid in the identification and characterization of mechanisms leading to brittle failure.

The following observations were made with respect to uniaxial testing performed on samples of pink Lac du Bonnet granite:

(1) Crack closure involved both axial and lateral strain components.

(2) Near-linear elastic behaviour was seen only in axial strain measurements. Lateral strain followed a nonlinear trend throughout the entire test, as depicted through continuously decreasing values of lateral stiffness.

(3) The combined use of moving point regression analysis (performed on the axial, lateral, and volumetric stress-strain curves) and acoustic emission response (including the event

Fig. 13. Plot of cumulative elastic impulse energy vs. axial stress and the stress-dependent energy rate vs. axial stress for a 130 Level pink granite.

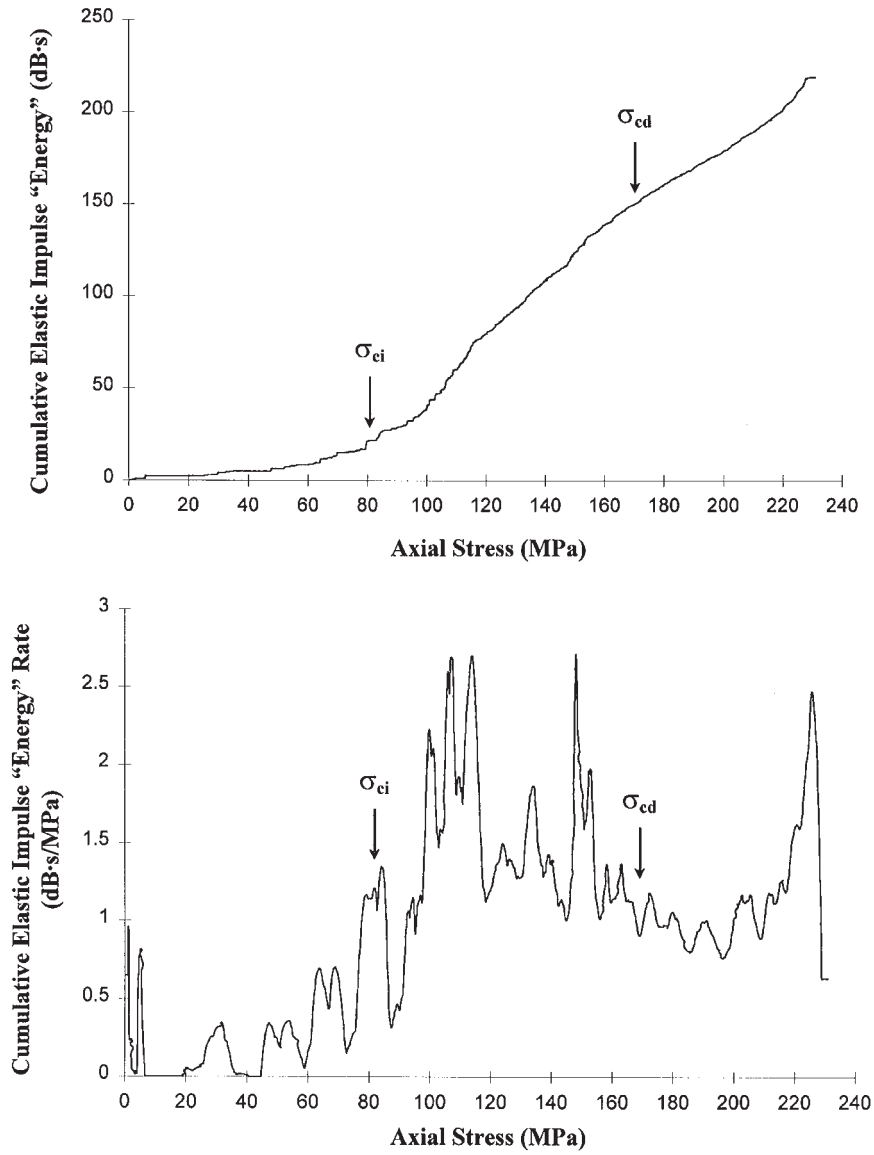
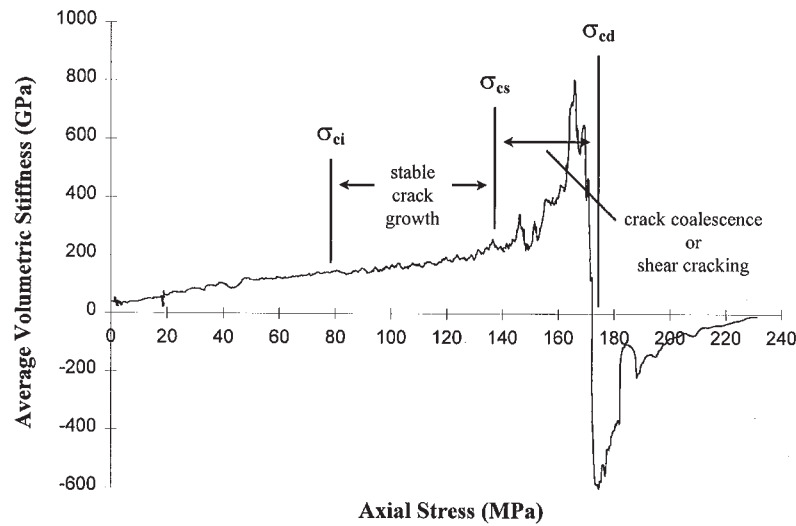


Fig. 14. Plot of average volumetric stiffness vs. axial stress, indicating the occurrence of major strain rate changes between crack initiation and crack damage for a 130 Level pink granite. σ_{cs} , crack coalescence stress threshold.



properties and energy calculations) provided the most accurate and reliable means of identifying crack initiation (σ_{ci}).

(4) Analysis of both the axial and lateral stiffness curves indicates that a significant rate change in strain occurs prior to the crack damage threshold, possibly marking the small-scale coalescence of cracks.

Acknowledgments

Parts of the work have been supported by Atomic Energy of Canada Limited and a Natural Sciences and Engineering Research Council of Canada operating grant. The authors wish to thank Dr. Derek Martin and Zig Szczepanik for their suggestions and contributions to this work. Special thanks are extended to Dr. Emery Lajtai for his insights into the initial stages of this work.

References

- Beattie, A.G. 1983. Acoustic emission, principles and instrumentation. *Journal of Acoustic Emission*, **2**(1/2): 95–128.
- Bieniawski, Z.T. 1967a. Mechanism of brittle rock fracture. Part I. Theory of the fracture process. *International Journal of Rock Mechanics and Mining Sciences & Geomechanical Abstracts*, **4**(4): 395–406.
- Bieniawski, Z.T. 1967b. Mechanism of brittle rock fracture. Part II. Experimental studies. *International Journal of Rock Mechanics and Mining Sciences & Geomechanical Abstracts*, **4**(4): 407–423.
- Brace, W.F. 1964. Brittle fracture of rocks. In *State of Stress in the Earth's Crust*, Proceedings of the International Conference, Santa Monica, Calif. Edited by W.R. Judd. American Elsevier Publishing Company, New York, pp. 110–178.
- Brace, W.F., and Bombolakis, E.G. 1963. A note on brittle crack growth in compression. *Journal of Geophysical Research*, **68**(12): 3709–3713.
- Brace, W.F., Paulding, B.W., Jr., and Scholz, C. 1966. Dilatancy in the fracture of crystalline rocks. *Journal of Geophysical Research*, **71**(16): 3939–3953.
- Cannon, N.P., Schulson, E.M., Smith, T.R., and Frost, H.J. 1990. Wing cracks and brittle compressive fracture. *Acta Metallurgica et Materialia*, **38**(10): 1955–1962.
- Eberhardt, E., Stead, D., and Szczepanik, Z. 1996. Crack initiation and propagation in granite and granodiorite from the 130 m and 420 m levels of the URL. Atomic Energy of Canada Limited, Report AECL 122567.
- Eberhardt, E., Stead, D., Stimpson, B., and Lajtai, E.Z. 1998. The effect of neighbouring cracks on elliptical crack initiation and propagation in uniaxial and triaxial stress fields. *Engineering Fracture Mechanics*, **59**(2): 103–115.
- Hardy, H.R., Jr. 1977. Emergence of acoustic emission/microseismic activity as a tool in geomechanics. In *Proceedings of the 1st Conference on Acoustic Emission/Microseismic Activity in Geologic Structures and Materials*, 1975, University Park, Pa. Edited by H.R. Hardy and L.W. Leighton. Trans Tech Publications, Clausthal, Germany, pp. 3–31.
- Hoek, E., and Bieniawski, Z.T. 1965. Brittle fracture propagation in rock under compression. *International Journal of Fracture Mechanics*, **1**(3): 137–155.
- Huang, J., Wang, Z., and Zhao, Y. 1993. The development of rock fracture from microfracturing to main fracture formation. *International Journal of Rock Mechanics and Mining Sciences & Geomechanical Abstracts*, **30**(7): 925–928.
- Jackson, R., and Lau, J.S.O. 1990. The effect of specimen size on the laboratory mechanical properties of Lac du Bonnet grey granite. In *Proceedings of the 1st International Workshop on Scale Effects in Rock Masses*, Loen, Norway. Edited by A. Pinto da Cunha. A.A. Balkema, Rotterdam, pp. 165–174.
- Khair, A.W. 1984. Acoustic emission pattern: an indicator of mode of failure in geologic materials as affected by their natural imperfections. In *Proceedings of the 3rd Conference on Acoustic Emission/Microseismic Activity in Geologic Structures and Materials*, 1981, University Park, Pa. Edited by H.R. Hardy, Jr., and F.W. Leighton. Trans Tech Publications, Clausthal, Germany, pp. 45–66.
- Lajtai, E.Z. 1971. A theoretical and experimental evaluation of the Griffith theory of brittle fracture. *Tectonophysics*, **11**: 129–156.
- Lajtai, E.Z., and Lajtai, V.N. 1974. The evolution of brittle fracture in rocks. *Journal of the Geological Society, London*, **130**(1): 1–18.
- Lajtai, E.Z., Carter, B.J., and Duncan, E.J.S. 1994. En echelon crack-arrays in potash salt rock. *Rock Mechanics and Rock Engineering*, **27**(2): 89–111.
- Lockner, D.A., Byerlee, J.D., Kukusenko, V., Ponomarev, A., and Sidorin, A. 1991. Quasi-static fault growth and shear fracture energy in granite. *Nature (London)*, **350**(6313): 39–42.
- Mansurov, V.A. 1994. Acoustic emission from failing rock behaviour. *Rock Mechanics and Rock Engineering*, **27**(3): 173–182.
- Martin, C.D. 1990. Characterizing *in situ* stress domains at the AECL Underground Research Laboratory. *Canadian Geotechnical Journal*, **27**: 631–646.
- Martin, C.D. 1993. The strength of massive Lac du Bonnet granite around underground openings. Ph.D. thesis, Department of Civil and Geological Engineering, University of Manitoba, Winnipeg, Man.
- Martin, C.D., and Chandler, N.A. 1994. The progressive fracture of Lac du Bonnet granite. *International Journal of Rock Mechanics and Mining Sciences & Geomechanical Abstracts*, **31**(6): 643–659.
- Nemat-Nasser, S., and Horii, H. 1982. Compression-induced nonplanar crack extension with application to splitting, exfoliation and rockburst. *Journal of Geophysical Research*, **87**(B8): 6805–6821.
- Ohnaka, M., and Mogi, K. 1982. Frequency characteristics of acoustic emissions in rocks under uniaxial compression and its relation to the fracturing process to failure. *Journal of Geophysical Research*, **87**(B5): 3873–3884.
- Peng, S., and Johnson, A.M. 1972. Crack growth and faulting in cylindrical specimens of Chelmsford granite. *International Journal of Rock Mechanics and Mining Sciences & Geomechanical Abstracts*, **9**(1): 37–86.
- Scholz, C.H. 1968. Microfracturing and the inelastic deformation of rock in compression. *Journal of Geophysical Research*, **73**(4): 1417–1432.
- Schulson, E.M., Kuehn, G.A., Jones, D.A., and Fifolt, D.A. 1991. The growth of wing cracks and the brittle compressive failure of ice. *Acta Metallurgica et Materialia*, **39**(11): 2651–2655.
- Spanner, J.C., Brown, A., Hay, D.R., Mustafa, V., Notvest, K., and Pollock, A. 1987. Fundamentals of acoustic emission testing. In *Nondestructive testing handbook: acoustic emission testing*. Edited by P. McIntire. American Society for Nondestructive Testing, Columbus, Ohio, pp. 11–61.
- Wawersik, W.R., and Fairhurst, C. 1970. A study of brittle rock fracture in laboratory compression experiments. *International Journal of Rock Mechanics and Mining Sciences & Geomechanical Abstracts*, **7**(5): 561–575.